

Crystalline Electric-Field Excitations in Quantum Spin Liquids Candidate NaYbSe₂

Zheng Zhang,^{1,2} Xiaoli Ma,¹ Jianshu Li,^{1,2} Guohua Wang,³ D.T. Adroja,^{4,5} T.G. Perring,⁴ Weiwei Liu,^{1,2} Feng Jin,¹ Jianting Ji,¹ Yimeng Wang,^{1,2} Xiaoqun Wang,³ Jie Ma,^{3,*} and Qingming Zhang^{6,1,†}

¹*Beijing National Laboratory for Condensed Matter Physics,*

Institute of Physics, Chinese Academy of Sciences, Beijing 100190, China

²*Department of Physics, Renmin University of China, Beijing 100872, China*

³*Department of Physics and Astronomy, Shanghai Jiao Tong University, Shanghai 200240, China*

⁴*ISIS Neutron and Muon Facility, SCFT Rutherford Appleton Laboratory, Chilton, Didcot Oxon, OX11 0QX, United Kingdom*

⁵*Highly Correlated Matter Research Group, Physics Department, University of Johannesburg, Auckland Park 2006, South Africa*

⁶*School of Physical Science and Technology, Lanzhou University, Lanzhou 730000, China*

Very recently we revealed a large family of triangular lattice quantum spin liquid candidates named rare-earth chalcogenides, which features a high-symmetry structure without structural/charge disorders and spin impurities, and may serve as an ideal platform exploring spin liquid physics. The knowledge of crystalline electric-field (CEF) excitations is an essential step to explore the fundamental magnetism of rare-earth spin systems. Here we employed inelastic neutron scattering (INS) and Raman scattering (RS) to carry out a comprehensive CFE investigation on NaYbSe₂, a promising representative of the family. By comparison with its nonmagnetic compound NaLuSe₂, we are able to identify the CEF excitations at 15.8, 24.3 and 30.5 meV at 5K. The selected cuts of the INS spectra are well re-produced with a large anisotropy of g factors ($g_{ab} : g_c \sim 3 : 1$). Further, the CEF excitations are explained well by our calculations based on the point charge model. Interestingly, NaYbSe₂ exhibits an unusual CEF shift to higher energies with increasing temperatures, and the Raman mode close to the first CEF excitation shows an anomalously large softening with decreasing temperatures. The absence of the anomalies in NaLuSe₂ clearly demonstrates a CEF-phonon coupling not reported in the family. It can be understood in term of the weaker electronegativity of Se. The fact that the smallest first CEF excitation in the sub-family of NaYbCh₂ is ~ 180 K (Ch=O, S, Se), guarantees that the sub-family can be strictly described with an effective $S=1/2$ picture at sufficiently low temperatures. Interestingly the CEF-phonon coupling revealed here may present alternative possibilities to manipulate the spin systems.

INTRODUCTION

Quantum spin liquid (QSL) is a novel quantum spin-entangled state breaking no symmetry even at zero temperature[1, 2]. The idea of QSL was proposed by P.W Anderson in 1973 and then applied to high temperature superconductivity[3, 4]. A lot of theoretical effort has been contributed to the exotic state since then. X.G.Wen made a topological classification for QLSs on the mean-field level[5]. In 2006, Kitaev proposed an exactly solvable model on a spin-1/2 honeycomb lattice, which inspires topological quantum computing based on strong spin-entanglement of QSL[6].

Meanwhile, much effort has also been made on the material side. Herbersmithite is a famous QSL candidate with 3d spin-1/2 Cu²⁺ ions sitting on the kagome lattice[7, 8], while the anti-site mixing between Cu²⁺ and Zn²⁺ ions remains a key issue in uncovering the intrinsic properties of the spin ground state. We turned to strong spin-orbital (SO) coupling and discovered the rare-earth-based QSL candidate YbMgGaO₄, which possesses a perfect spin triangular lattice and rules out the anti-site mixing, spin impurities and Dyaloshinski-Moriya interaction [9, 10]. A series of experiments down to milikelvins, such as thermodynamic measurements, muon spin relax-

ation (μ SR) and INS etc., consistently suggest a gapless QSL ground state[10–14]. On the other hand, it was concerned that the charge disorder between Mg/Ga in YbMgGaO₄[15] may have influence on the spin channel.

The idea of strong SO coupling continuously leads us to reveal a large family of rare-earth-based QSL candidates ARECh₂ (A=Alkali or monovalent ion, RE=rare earth, Ch=chalcogen)[16]. The family shares the same high symmetry with YbMgGaO₄ and inherits almost all the advantages of it but naturally removes the issue of charge disorder. Most excitingly, the family has a huge diversity of members and the preliminary results show that the antiferromagnetic (AF) exchange coupling is improved by at least one order of magnitude compared to YbMgGaO₄. These enable the family as a unique and ideal playground for spin liquid study.

The exploration on the sub-family of NaYbCh₂ (Ch=chalcogen) has been launched[16–28]. The knowledge of the CFE excitations is an essential step to look into the fundamental magnetism of the family. Among the NaYbCh₂ members, NaYbSe₂ is of particular interest since it shows a distinct QSL signature and an appropriate charge gap (~ 1.92 eV) which is crucial to the metallization and material engineering[16]. Another interesting issue is the essential influence of the ligand anions on structural and magnetic properties, for which

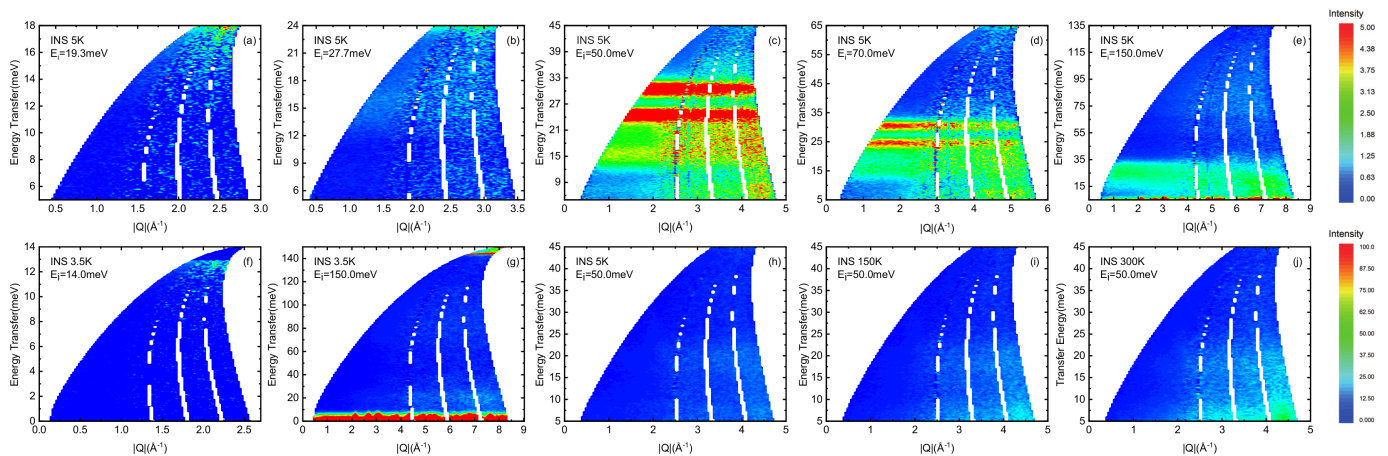


FIG. 1. Upper panel: INS spectra of NaYbSe₂ measured with different incident neutron energies at 5K. Lower panel: INS spectra of non-magnetic NaLuSe₂ for comparison.

we expect to find some key clues by investigating the CEF excitations of NaYbSe₂. At present we are able to grow NaYbSe₂ single crystals with the largest dimension (~ 20 mm) among the sub-family members. This makes single-crystal neutron scattering experiments possible and it is highly required to figure out the CEF excitations of NaYbSe₂ before inelastic neutron scattering experiments.

In this paper, by applying INS and RS to NaYbSe₂ and its nonmagnetic reference compound NaLuSe₂, we made a comprehensive investigation on the CEF excitations in NaYbSe₂ that revealed an unusual CEF-Phonon coupling. Three CEF excitations, at 15.79meV, 24.33meV and 30.53meV, are probed at 5K by INS experiments, and further confirmed by RS experiments. Our simulations well re-produce the selected cuts of the INS spectra and we employed the point charge model to calculate the CEF excitations which are consistent with the experimental ones. Both INS and RS experiments demonstrate that the CEF excitations unexpectedly shift to higher energies with increasing temperatures. Moreover, the Raman phonon mode very close to the first CEF excitation is significantly softened with decreasing temperatures and its width also shows an abnormal behavior, while the anomalies completely disappear in NaLuSe₂. These allow to identify a CEF-phonon coupling in NaYbSe₂. The phonon anomalies as well as the unusual CEF temperature dependence, can be explained in term of the electronegativity of chalcogen elements.

EXPERIMENTAL TECHNIQUES

The high-quality single crystals of NaYbSe₂, as well as the nonmagnetic NaLuSe₂, were grown using a NaCl-flux method. The single crystals with the dimensions of 5mm \times 5mm were used in RS experiments. The poly-

crystalline NaYbSe₂ and NaLuSe₂ were synthesized by the high-temperature solid state reaction and were characterized to be single-phased[16]. ~ 5 g powder sample of NaYbSe₂ and ~ 3 g powder sample of NaLuSe₂ were used in INS experiments (See supplementary materials for details). The INS data on NaYbSe₂ and nonmagnetic reference compound NaLuSe₂ were collected using the high flux and high resolution time of flight spectrometers, MAPS, at the ISIS pulsed neutron facility, Rutherford Appleton Laboratory, U.K. The energy- and temperature-dependence of data were obtained. The powder samples were loaded in a cylinder Al-can with an inner diameter of 30mm. The closed cycle refrigerator (CCR) was used to cool the samples to a based temperature of 5K with He-exchange gas. The Raman spectra were collected using a HR800 (Jobin Yvon) and T64000 (Jobin Yvon) equipped with a 633nm and 473nm laser, charge-coupled device(CCD) and volume Bragg gratings. After cleavage, the single crystals of NaYbSe₂ and NaLuSe₂ were placed in a closed-cycle cryostat for Raman experiments. Backscattering configuration was employed and the polarizations of both incident and scattering light lie in the ab plane.

CEF EXCITATIONS AND INELASTIC NEUTRON SCATTERING

The INS spectra for NaYbSe₂ with the incident neutron energy $E_i = 19.3, 27.7, 50.0, 70.0$ and 150.0 meV at 5K are shown in Fig. 1 (upper panel). Three excitations can be clearly seen at 15.8, 24.3 and 30.5 meV, respectively. For comparison, the INS spectra of nonmagnetic reference sample NaLuSe₂ are also shown here (lower panel of Fig. 1) and only weak phonon excitations are observed. We have the similar observations in Raman experiments. In Raman channel, the excita-

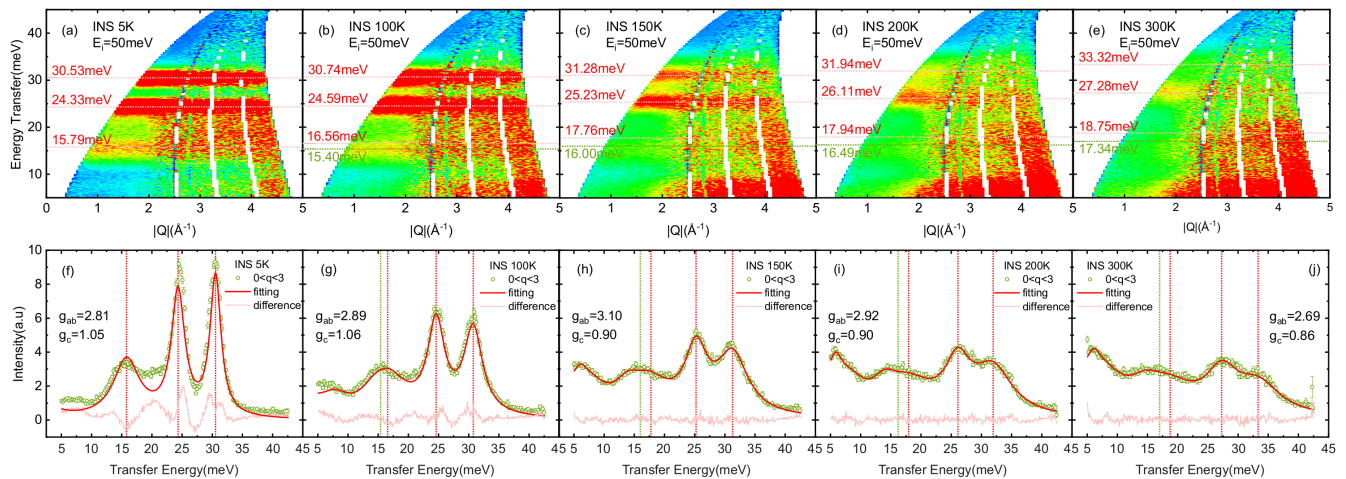


FIG. 2. (a)~(e) are the INS spectra for NaYbSe₂ measured with the incident neutron energy $E_i = 50$ meV at selected temperatures. (f)~(j) are the cuts of INS intensity versus energy corresponding to (a)~(e). The data in (f)~(j) are obtained by integrating over the wavevector space from 0 to 3 \AA^{-1} (green dots). The fitting curves (red lines) are given by multiple iterations with initial CEF parameters calculated from the point charge model. In (a)~(e) and (f)~(j), the fitted 1st, 2nd and 3rd CEF excitations of Yb³⁺ are highlighted by dashed red lines. The dashed green lines above 100 K mark E_g phonon mode which is identified in Raman experiments.

tions are observed in NaYbSe₂ while they are absent in NaLuSe₂. The observed excitations exhibit the momentum-independence and their absence in NaLuSe₂, which rule out the phononic origin of them, and hence can be unambiguously identified as the CEF ones.

It is interesting that the first CEF excitation of 15 meV (~ 185 K) is smaller than that of YbMgGaO₄ (39meV, ~ 480 K)[15] and that of NaYbO₂ (36meV, ~ 440 K)[19]. It suggests that the larger Se-Yb bond length and the weaker electronegativity of selenium effectively reduce the CEFs at Yb ions. The first CEF excitation sets a fundamental energy scale for studying the magnetism of NaYbSe₂ and allows to make a relatively accurate Curie-Weiss analysis.

Fig. 2 demonstrates the temperature dependence of the CEF excitations. The cuts of the integrated spectra in the ranges of low wavevector ($0 \sim 3 \text{\AA}^{-1}$) and high wavevector ($3 \sim 5 \text{\AA}^{-1}$) are shown in Fig.2(f) ~ 2(j). There are several points we can draw from the spectra.

(i) The intensity of the three CEF excitations decrease with $|Q|$. This can be explained by the magnetic form factor $F(|Q|)$ related to magnetic ions in the differential neutron scattering cross section. We calculated the magnetic form factor $F^2(|Q|)$ as a function of $|Q|$, and found that the scattering intensity decreases with increasing $|Q|$, consistent with the observations here (See supplementary material).

(ii) The intensity of the CEF excitations decreases with increasing temperature. This simply comes from the population factor and thermal broadening and the similar behavior has been also seen in YbMgGaO₄[15] and NaYbS₂[17].

(iii) Most interestingly, the CEF excitations exhibit a slight but clear shift to higher energies with increasing temperatures. Our Raman experiments also catch the shift (Fig. 4). This unusual temperature dependence was not observed in YbMgGaO₄[15] and NaYbS₂[17]. The temperature-dependent CEF excitations are quite unusual. This seems related to the larger radius of Se anion or its weaker electronegativity. At lower temperatures, there is a larger overlap of electron cloud between Yb and Se, which reduces the effective charges of Se anions and hence gives rise to the lower CEF levels based on the point charge model. With increasing temperatures, the general lattice expansion slightly but continuously enlarges the bond distance between Yb and Se and reduces the electron cloud overlap between them. This slightly enhances the ionicity of the compound and raises the effective charge of Se, and consequently lifts the CEF levels in a small amount. The thermal broadening of the CEF levels at higher temperatures actually makes the lift obscure, as observed in neutron experiments.

(iv) The first CEF energy level above 100 K deviates from the fitted one (FIG. 2(f) ~ 2(j)). This may be related to the coupling between CEF excitations and phonons. The CEF excitations move towards high energy with increasing temperatures, while the coupling enables an energy exchange between the first CEF excitation and phonons which are very close in energy (See below). Eventually the first CEF excitation exhibits a smaller shift with temperature compared to the second and third excitations. The effect is also seen by RS experiments (See below). In the reference sample NaLuSe₂, only one broad peak has been observed and the its posi-

tion decreases with increasing temperatures (See supplementary material). It can be identified as a phonon mode through our RS experiments.

We have determined the CEF parameters by carefully fitting the cuts of INS spectra in the range from 0 to 3 \AA^{-1} . The fitting details and the extracted CEF parameters can be found in the supplementary materials. The CEF parameters can be calculated by using formulas (See supplementary material). The calculated g-factors are shown in the panel of Fig. 2(f) \sim 2(j). The ratio of $g_{ab\text{-plane}}$ to $g_{c\text{-axis}}$ is $\sim 3:1$, close to that in NaYbO_2 and NaYbS_2 [17, 18]. This indicates that the sub-family AYbCh_2 has a systematic and strong magnetic anisotropy, which is much less in YbMgGaO_4 where the ratio is close to 1 [9]. The difference may stem from the charge imbalance of different cations between Yb^{3+} layers [29].

We have calculated the CEF levels in NaYbO_2 , NaYbS_2 and NaYbSe_2 using the point charge model (See supplementary materials), and made comparison with the experimental ones (Fig. 3). Generally the CEF levels decrease with the radii of O, S and Se as expected. One can see a good agreement between experiments and calculations for the first CEF level. The calculated first CEF levels are $\sim 39.7 \text{ meV}$ (NaYbO_2), $\sim 20.2 \text{ meV}$ (NaYbS_2), and $\sim 16.52 \text{ meV}$ (NaYbSe_2), and the experimental values obtained from INS measurements are 34.8 meV [19], 17 meV [17], and 15.8 meV , respectively. It implies that the ionic crystal picture still works well even for the case with larger selenium anions. When we look at the second and third excitation levels, there is a relatively

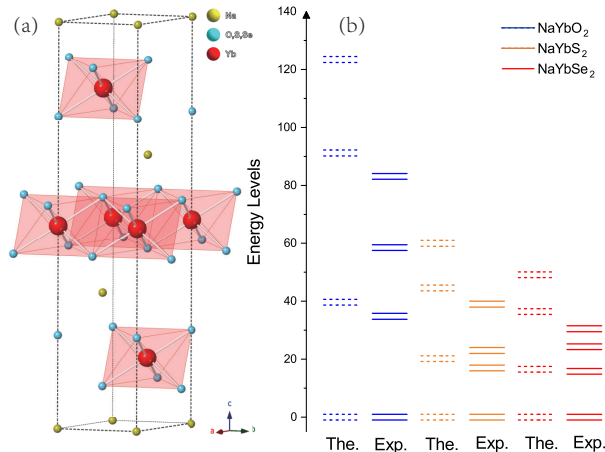


FIG. 3. (a) Crystal structure of AYbCh_2 ($\text{Ch}=\text{O}, \text{S}, \text{Se}$). (b) Experimental CEF excitation energy levels extracted from INS experiments (solid lines) and the calculated ones based on the point charge model (dashed lines).

large discrepancy between the experimental and calculated ones. Reducing the discrepancy actually requires a higher-order and accurate description on the CEF environments. The results also suggest that though the magnetism in the QSL candidates is dominated by rare-earth magnetic ions, the surrounding coordination anions (O, S and Se etc.) and the cations between magnetic planes have impact on spin states.

CEF-PHONON COUPLING AND RAMAN SCATTERING

Fig. 4 shows Raman spectra of NaYbSe_2 and NaLuSe_2 . The crystal symmetry $R-3m$ allows two Raman-active phonon modes $A_g + E_g$. Symmetry analysis indicates that $[A_g]$ mode is visible only in the parallel polarization configuration while E_g mode can be observed for in both parallel and cross polarization configurations. The two modes can be clearly identified with the polarized spectra in Fig. 4(a) and 4(b).

Besides the Raman modes, two weaker bands appear at 217 and 277 cm^{-1} in the spectra of NaYbSe_2 . The frequencies exactly match the 2nd and 3rd CEF levels given by INS measurements. And the bands completely disappear in NaLuSe_2 . Therefore, the two bands can be safely assigned to the CEF excitations. In fact, Raman scattering is a unique method to probe CEF excitations and has been applied to many rare-earth-based spin systems $\text{Tb}_2\text{Ti}_2\text{O}_7$ [30–32]. It is worth noting that the intensities of the two bands are quite different in the parallel and cross polarization configurations. This may be related to the strong anisotropy in NaYbSe_2 .

There are several obvious anomalies in the Raman spectra of NaYbSe_2 : 1) phonon mode broadening; 2) asymmetric lineshape of E_g mode; 3) particularly E_g mode shows a completely unusual softening with decreasing temperatures (Fig. 4(d)), and its width also has an abnormal temperature dependence (Fig. 4(e)). In contrast, all the anomalies are absent in the non-magnetic reference compound NaLuSe_2 . This unambiguously points to a magnetic origin. Spin-phonon coupling can be ruled out, because the broadening and asymmetry of E_g mode already exist even at room temperature which is almost one order of magnitude larger than exchange coupling. Thus we can identify that the anomalies stem from the CEF-phonon coupling. This is strongly supported by the fact that the energy scales of the CEF excitations exactly overlap with phonon frequencies. Particularly for E_g mode, its frequency is very close to the first CEF level, though the first excitation is too weak to be observed in Raman channel perhaps due to its quite large broadening as seen in INS measurements (Fig. 2). The CEF-phonon coupling has been reported in many rare-earth compounds [30, 32, 33]. It may provide alternative possibility to tune the CEF excitations and the

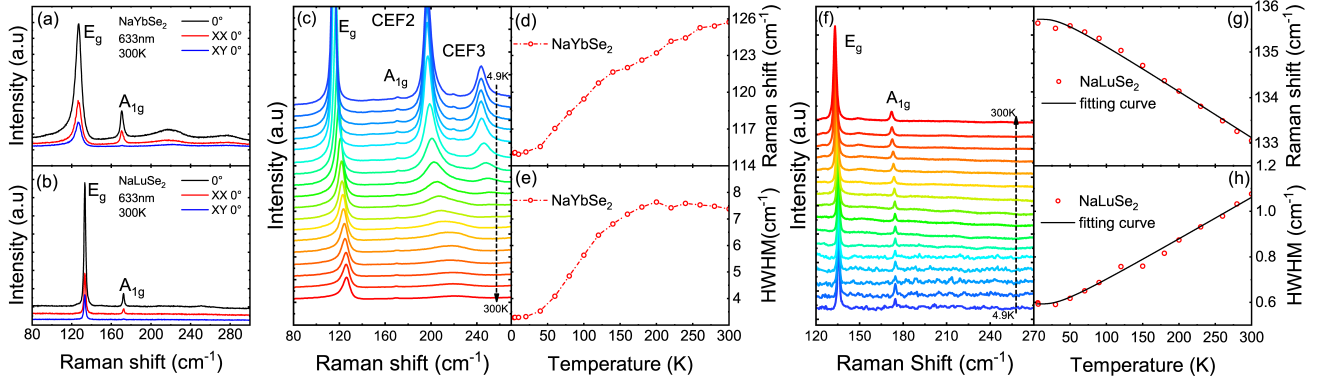


FIG. 4. Polarized Raman spectra for NaYbSe₂ (a) and NaLuSe₂ (b). XX and XY represent parallel and cross polarization configurations, respectively. (c) and (f) are the temperature-dependent Raman spectra of NaYbSe₂ and NaLuSe₂, respectively, and the Raman shift and half widths at half-maximum (HWHM) of E_g mode are shown in panle (d), panle (e) and panle (g), panle (h).

magnetism of the rare-earth spin system.

The CEF-phonon coupling is considered to share the similar origin resulting in the unusual CEF temperature dependence as discussed above, and involve the degeneracy of the first CEF excitation and E_g mode. The larger electron cloud overlap between Yb and Se in principle gives rise to a CEF-phonon coupling. The coupling in NaYbSe₂ is dramatically magnified by the resonance-like effect, which originates from the fact that the first CEF excitation and E_g mode are very close in energy. More precisely, the first CEF excitation is only ~ 1 meV higher than the phonon energy at room temperature. With decreasing temperatures, the phonon frequency normally goes up while the first CEF level goes down as discussed above. The tiny energy discrepancy will be immediately filled and the resonance-like effect occurs. Generally the effect splits the resonance energy into the lower (phonon) and upper (CEF) branches. This effectively gives a phonon softening. The first CEF level seems to be dominated by the enhancement of Se electronegativity and remains decreasing with lowering temperatures.

CONCLUSION

The CEF excitations of Yb³⁺ in NaYbSe₂ have been comprehensively studied using INS and Raman experiments and by comparison with non-magnetic reference sample NaLuSe₂. Three CEF excitations are observed by INS experiments and the cuts of INS spectra are well simulated to extract the CEF parameters. Based on the point charge model, we are able to reproduce the CEF excitations of NaYbO₂, NaYbS₂ and NaYbSe₂, which are well consistent with the existing experimental observations.

Despite the common characteristics of the sub-family NaYbCh₂, NaYbSe₂ exhibits some unique features in the CEF excitations compared to NaYbO₂ and NaYbS₂. One is that the observed CEF excitations show an interesting shift to higher energies with increasing temperatures. This is naturally understood in term of electronegativity. Another one is the obvious CEF-phonon coupling. The comparison of INS spectra of NaYbSe₂ and NaLuSe₂, allow us to identify a phonon mode around 15 meV, which is very close to the first CEF excitation of NaYbSe₂. We double-checked the CEF excitations and the phonon mode in Raman channel. Surprisingly, the E_g phonon mode close to the first CEF excitation shows a large softening with decreasing temperatures, while the same mode in NaLuSe₂ has a normal hardening. The contrast is a clear demonstration of CEF-phonon coupling. The unusual CEF temperature dependence stems from the weaker electronegativity which, combined with the resonance-like process, also explains the anomalous phonon softening.

This work was supported by the Ministry of Science and Technology of China (2017YFA0302904 & 2016YFA0300500) and the NSF of China (11774419 & U1932215). The data processing of INS spectrum in FIG. 1 and FIG. 2 are based on mantid software[34, 35]. The CEF energy levels calculation is based on our own MATLAB program. The theoretical calculation of CEF based on point charge model is also based on mantid software[34, 35]. We thank the Ross Stewart for help on MAPS and ISIS Facility for beam time, RB1910575. The experimental data can be found at <https://doi.org/10.5286/ISIS.E.RB1910575-1>

* e-mail:jma3@sztu.edu.cn

† e-mail:qmzhang@ruc.edu.cn

- [1] L. Balents, Spin liquids in frustrated magnets, *Nature* **464**, 199 (2010).
- [2] L. Savary and L. Balents, Quantum spin liquids: a review, *Rep. Prog. Phys.* **80**, 016502 (2016).
- [3] P. Anderson, Resonating valence bonds: A new kind of insulator?, *Mater. Res. Bull.* **8**, 153 (1973).
- [4] P. W. Anderson, The resonating valence bond state in La_2CuO_4 and superconductivity, *Science* **235**, 1196 (1987).
- [5] X. G. Wen, Mean-field theory of spin-liquid states with finite energy gap and topological orders, *Phys. Rev. B* **44**, 2664 (1991).
- [6] A. Kitaev, Anyons in an exactly solved model and beyond, *Ann. Phys.* **321**, 2 (2006).
- [7] M. P. Shores, E. A. Nytko, B. M. Bartlett, and D. G. Nocera, A structurally perfect $s=1/2$ kagomé antiferromagnet, *J. Am. Chem. Soc.* **127**, 13462 (2005).
- [8] T.-H. Han, J. S. Helton, S. Chu, D. G. Nocera, J. A. Rodriguez-Rivera, C. Broholm, and Y. S. Lee, Fractionalized excitations in the spin-liquid state of a kagome-lattice antiferromagnet, *Nature* **492**, 406 (2012).
- [9] Y. Li, G. Chen, W. Tong, L. Pi, J. Liu, Z. Yang, X. Wang, and Q. Zhang, Rare-earth triangular lattice spin liquid: A single-crystal study of YbMgGaO_4 , *Phys. Rev. Lett.* **115** (2015).
- [10] Y. Li, H. Liao, Z. Zhang, S. Li, F. Jin, L. Ling, L. Zhang, Y. Zou, L. Pi, Z. Yang, J. Wang, Z. Wu, and Q. Zhang, Gapless quantum spin liquid ground state in the two-dimensional spin-1/2 triangular antiferromagnet YbMgGaO_4 , *Sci. Rep.* **5** (2015).
- [11] Y. Li, D. Adroja, P. K. Biswas, P. J. Baker, Q. Zhang, J. Liu, A. A. Tsirlin, P. Gegenwart, and Q. Zhang, Muon spin relaxation evidence for the $u(1)$ quantum spin-liquid ground state in the triangular antiferromagnet YbMgGaO_4 , *Phys. Rev. Lett.* **117** (2016).
- [12] Y. Li, D. Adroja, D. Voneshen, R. I. Bewley, Q. Zhang, A. A. Tsirlin, and P. Gegenwart, Nearest-neighbour resonating valence bonds in YbMgGaO_4 , *Nat. Commun.* **8** (2017).
- [13] Y. Shen, Y.-D. Li, H. Wo, Y. Li, S. Shen, B. Pan, Q. Wang, H. C. Walker, P. Steffens, M. Boehm, Y. Hao, D. L. Quintero-Castro, L. W. Harriger, M. D. Frontzek, L. Hao, S. Meng, Q. Zhang, G. Chen, and J. Zhao, Evidence for a spinon fermi surface in a triangular-lattice quantum-spin-liquid candidate, *Nature* **540**, 559 (2016).
- [14] Y. Li, YbMgGaO_4 : A triangular-lattice quantum spin liquid candidate, *Adv. Quantum Technol.* **2**, 1900089 (2019).
- [15] Y. Li, D. Adroja, R. I. Bewley, D. Voneshen, A. A. Tsirlin, P. Gegenwart, and Q. Zhang, *Phys. Rev. Lett.* **118**, 107202 (2017).
- [16] W. Liu, Z. Zhang, J. Ji, Y. Liu, J. Li, X. Wang, H. Lei, G. Chen, and Q. Zhang, Rare-earth chalcogenides: A large family of triangular lattice spin liquid candidates, *Chin. Phys. Lett.* **35**, 117501 (2018).
- [17] M. Baenitz, P. Schlender, J. Sichelschmidt, Y. A. Onykiienko, Z. Zangeneh, K. M. Ranjith, R. Sarkar, L. Hozoi, H. C. Walker, J.-C. Orain, H. Yasuoka, J. van den Brink, H. H. Klauss, D. S. Inosov, and T. Doert, NaYbS_2 : A planar spin-1/2 triangular-lattice magnet and putative spin liquid, *Phys. Rev. B* **98**, 220409 (2018).
- [18] K. M. Ranjith, D. Dmytriieva, S. Khim, J. Sichelschmidt, S. Luther, D. Ehlers, H. Yasuoka, J. Wosnitza, A. A. Tsirlin, H. Khne, and M. Baenitz, Field-induced instability of the quantum spin liquid ground state in the $jeff=12$ triangular-lattice compound NaYbO_2 , *Phys. Rev. B* **99** (2019).
- [19] L. Ding, P. Manuel, S. Bachus, F. Grubler, P. Gegenwart, J. Singleton, R. D. Johnson, H. C. Walker, D. T. Adroja, A. D. Hillier, and A. A. Tsirlin, Gapless spin-liquid state in the structurally disorder-free triangular antiferromagnet NaYbO_2 , *Phys. Rev. B* **100** (2019).
- [20] J. Sichelschmidt, P. Schlender, B. Schmidt, M. Baenitz, and T. Doert, Electron spin resonance on the spin-1/2 triangular magnet NaYbS_2 , *J. Phys.: Condens. Matter* **31**, 205601 (2019).
- [21] K. M. Ranjith, S. Luther, T. Reimann, B. Schmidt, P. Schlender, J. Sichelschmidt, H. Yasuoka, A. M. Strydom, Y. Skourski, J. Wosnitza, H. Khne, T. Doert, and M. Baenitz, Anisotropic field-induced ordering in the triangular-lattice quantum spin liquid NaYbSe_2 , *Phys. Rev. B* **100** (2019).
- [22] J. Xing, L. D. Sanjeeva, J. Kim, G. R. Stewart, M.-H. Du, F. A. Reboledo, R. Custelcean, and A. S. Sefat, Crystal synthesis and frustrated magnetism in triangular lattice CsRESe_2 ($\text{RE} = \text{La}-\text{Lu}$): Quantum spin liquid candidates CsCeSe_2 and CsYbSe_2 , *Mater. Lett.* **71** (2019).
- [23] M. M. Bordelon, E. Kenney, C. Liu, T. Hogan, L. Posthuma, M. Kavand, Y. Lyu, M. Sherwin, N. P. Butch, C. Brown, M. J. Graf, L. Balents, and S. D. Wilson, Field-tunable quantum disordered ground state in the triangular-lattice antiferromagnet NaYbO_2 , *Nat. Phys.* **15**, 1058 (2019).
- [24] J. Xing, L. D. Sanjeeva, J. Kim, W. R. Meier, A. F. May, Q. Zheng, R. Custelcean, G. R. Stewart, and A. S. Sefat, Synthesis, magnetization, and heat capacity of triangular lattice materials NaErSe_2 and KErSe_2 , *Phys. Rev. Mater.* **3** (2019).
- [25] J. Xing, L. D. Sanjeeva, J. Kim, G. R. Stewart, A. Podlesnyak, and A. S. Sefat, Field-induced magnetic transition and spin fluctuations in the quantum spin-liquid candidate CsYbSe_2 , *Phys. Rev. B* **100** (2019).
- [26] S. Gao, F. Xiao, K. Kamazawa, K. Ikeuchi, D. Biner, K. Krmer, C. Regg, and T. hisa Arima, Crystal-electric-field excitations in a quantum-spin-liquid candidate NaErS_2 , <http://arxiv.org/abs/1911.10662v1>.
- [27] J. Sichelschmidt, B. Schmidt, P. Schlender, S. Khim, T. Doert, and M. Baenitz, Effective spin-1/2 moments on a Yb^{3+} triangular lattice: an esr study, <http://arxiv.org/abs/1912.01868v1>.
- [28] R. Sarkar, P. Schlender, V. Grinenko, E. Haeussler, P. J. Baker, T. Doert, and H. H. Klauss, Quantum spin liquid ground state in the disorder free triangular lattice NaYbS_2 , <http://arxiv.org/abs/1911.08036v1>.
- [29] Z. Zangeneh, S. Avdoshenko, J. van den Brink, and L. Hozoi, Single-site magnetic anisotropy governed by interlayer cation charge imbalance in triangular-lattice AYbX_2 , *Phys. Rev. B* **100** (2019).
- [30] G. Gntherodt, A. Jayaraman, G. Batlogg, M. Croft, and E. Melczer, Raman scattering from coupled phonon and electronic crystal-field excitations in CeAl_2 , *Phys. Rev. Lett.* **51**, 2330 (1983).
- [31] M. Maczka, M. L. Sanjuán, A. F. Fuentes, K. Hermanow-

- icz, and J. Hanuza, Temperature-dependent raman study of the spin-liquid pyrochlore $\text{Tb}_2\text{Ti}_2\text{O}_7$, *Phys. Rev. B* **78** (2008).
- [32] A. Sethi, J. Slimak, T. Kolodiazny, and S. Cooper, Emergent vibronic excitations in the magnetodielectric regime of Ce_2O_3 , *Phys. Rev. Lett.* **122** (2019).
- [33] K. Hense, E. Gratz, H. Nowotny, and A. Hoser, Lattice dynamics and the interaction with the crystal electric field in NdCu_2 , *J. Phys.: Condens. Matter* **16**, 5751 (2004).
- [34] O. Arnold, J. Bilheux, J. Borreguero, A. Buts, S. Campbell, L. Chapon, M. Doucet, N. Draper, R. F. Leal, M. Gigg, V. Lynch, A. Markvardsen, D. Mikkelsen, R. Mikkelsen, R. Miller, K. Palmén, P. Parker, G. Passos, T. Perring, P. Peterson, S. Ren, M. Reuter, A. Savici, J. Taylor, R. Taylor, R. Tolchenov, W. Zhou, and J. Zikovsky, Mantid-data analysis and visualization package for neutron scattering and μsr experiments, *Nucl. Instrum. Methods. Phys. Res. A* **764**, 156 (2014).
- [35] M. Andrew, R. Applin, O. Arnold, A. Bamidele, L. Basso, J. Borreguero, E. Brown, H. Brown, N. Draper, M. Ganeva, M. A. Gigg, G. Guest, S. Hahn, S. Heybrock, A. J. Jackson, S. Jenkins, S. Jones, D. Le, R. Leal, A. Lim, J. Lin, V. Lynch, M. McDonnell, G. Miladinovic, L. Moore, D. Nixon, E. Oram, P. F. Peterson, V. Reimund, A. Russell, H. Saunders, A. Savici, A. Soinen, A. Sokolova, B. Sullivan, D. Tasev, T. Titcombe, R. Tolchenov, G. Vardanyan, R. Whitfield, and W. Zhou, Mantid 4.1.0: Manipulation and analysis toolkit for instrument data (2019).